



Feasibility of perfusion and early-uptake ^{18}F -FDG PET/CT in primary hepatocellular carcinoma: a dual-input dual-compartment uptake model

Shaobo Wang^{1,2} · Boqiao Li^{3,4} · Pengfei Li⁵ · Ran Xie⁶ · Quanshi Wang⁷ · Hong Shi¹ · Jianfeng He^{3,4}

Received: 25 February 2021 / Accepted: 17 May 2021 / Published online: 2 June 2021
© Japan Radiological Society 2021

Abstract

Purpose PET enables a concurrent evaluation of perfusion status and metabolic activity. We aimed to evaluate the feasibility of perfusion and early-uptake ^{18}F -FDG PET/CT in hepatocellular carcinoma (HCC) using a dual-input dual-compartment uptake model.

Materials and methods Data from 5 min dynamic PET/CT and conventional PET/CT scans were retrospectively collected from 17 pathologically diagnosed HCCs. Parameters such as hepatic arterial blood flow (F_a), portal vein blood flow (F_v), total blood flow (F), hepatic arterial perfusion index (HPI), portal vein perfusion index (PPI), blood volume (BV), extracellular mean transit time (MTT) and intracellular uptake rate (K_i) were calculated. F_a , HPI , MTT and K_i images were generated and used to identify HCC.

Results Compared with the surrounding liver tissue, HCCs showed significant increases in F_a , HPI , K_i and the maximum standard uptake value (SUV_{max}) (all $P < 0.001$) and significant reductions in F_v ($P < 0.05$) and PPI ($P < 0.001$). F , BV and MTT (all $P > 0.05$) did not differ significantly between HCCs and the surrounding liver tissue. Perfusion and early-uptake PET/CT increased the positivity rate of HCCs from 52.9% with conventional PET/CT alone to 88.2% with the combined method ($P < 0.05$).

Conclusions Perfusion and early-uptake PET/CT are feasible for diagnosing HCC and provide added functional information to enhance diagnostic performance.

Keywords Positron-emission tomography · Perfusion imaging · Liver neoplasms

Shaobo Wang and Boqiao Li contributed equally to this work.

✉ Quanshi Wang
wqslph@vip.tom.com

✉ Hong Shi
shih@kust.edu.cn

✉ Jianfeng He
jfenghe@foxmail.com

¹ Yunnan Key Laboratory of Primate Biomedical Research, Institute of Primate Translational Medicine, Kunming University of Science and Technology, 727 South Jingming Rd., Kunming, Yunnan, China

² PET/CT Center, First People's Hospital of Yunnan, 157 Jinbi Rd., Kunming, Yunnan, China

³ Faculty of Information Engineering and Automation, Kunming University of Science and Technology, 727 South Jingming Rd., Kunming, Yunnan, China

⁴ Yunnan Key Laboratory of Artificial Intelligence, Kunming University of Science and Technology, Kunming, Yunnan, China

⁵ Faculty of Clinical Medicine, Dali University, 2 Hongsheng Rd, Dali, Yunnan, China

⁶ PET/CT Center, Yunnan Cancer Hospital, 519 Kunzhou Rd, Kunming, Yunnan, China

⁷ Nanfang PET Center, Nanfang Hospital of Southern Medical University, North Guangzhou Avenue, Guangzhou 1838, Guangdong, China

Introduction

According to the International Agency for Research on Cancer, liver cancer was predicted to be the sixth most commonly diagnosed cancer and fourth leading cause of cancer death worldwide in 2018, and primary hepatocellular carcinoma (HCC) comprises 75–85% of cases [1].

Although conventional ultrasonography (US), CT and magnetic resonance imaging (MR) are primarily performed to diagnose HCC, they are insufficient in assessing functional and molecular information. Perfusion imaging, which measures vascular physiology and pharmacokinetics, is a promising functional technique to assess the proliferation status, histological grades, microvascular density and efficacy of various anticancer therapies, predict early responses to anticancer treatments, detect tumors with negative findings on conventional imaging, and monitor tumor recurrence after therapy [2, 3].

2-Deoxy-2-(^{18}F) fluoro-D-glucose (^{18}F -FDG) positron-emission tomography (PET) or PET/computed tomography (CT) seems to be an effective noninvasive and functional modality for evaluating tumor glucose uptake and diagnosing most tumors. However, conventional ^{18}F -FDG PET/CT has a low positivity rate (36–70%) in the diagnosis of HCC, and different supplements are used to solve this issue at different PET or PET/CT centers. Novel radiotracers, including ^{11}C -labeled acetate, ^{11}C -labeled choline, N-(2- ^{18}F -fluoro-propionyl)-L-glutamate and ^{89}Zr -conjugated monoclonal antibodies against glypican-3, enhance the ability to diagnose HCC, similar to early dynamic and delayed PET/CT [4–6].

Compared with perfusion imaging using US, CT and MR, perfusion PET or PET/CT has some potential advantages in diagnosing HCC. First, PET enables concurrent evaluation of the perfusion status and metabolic activity using a single imaging modality, with no additional ^{18}F -FDG [6, 7]. Second, an extremely low dose of the glucologue ^{18}F -FDG is almost free from allergy and toxicity, allowing patients with contraindications to undergo US, CT and/or MR, including those with contrast allergies, hyperthyroidism, renal comorbidities, unstable angina pectoris, heart failure, implanted electronic devices and certain ferromagnetic metal implants [5]. Third, PET has a larger z-axis and lower radiation dose (average: 5.7 mSv with 4.3 MBq/kg of ^{18}F -FDG [8]) than perfusion CT (average: 11.5 mSv using 64-section multidetector CT [9]). Additionally, PET features a more proportional relationship between the imaging signal and tissue tracer concentration than MRI [10].

Estimating tumor blood flow from early dynamic ^{18}F -FDG PET/CT was first proposed by Mullani et al. [11, 12]. Three blood flow parameters [hepatic arterial perfusion

index (*HPI*), time to peak (*TTP*), and peak intensity (*PI*)] have been estimated to discriminate and characterize HCCs using a maximum-slope method [7]. A limitation of the method is that relatively few perfusion parameters are captured. Additionally, intracellular ^{18}F -FDG uptake occurs in early dynamic PET/CT [6] but has not been considered within the assumptions of the method.

A dual-input dual-compartment uptake model for analyzing dynamic gadoteric acid (Gd-EOB-DTPA) MRI helps capture additional perfusion parameters and permits intracellular tracer uptake [6, 13]; however, whether this model can be applied to the analysis of early dynamic ^{18}F -FDG PET/CT is unclear. In this preliminary study, we aimed to evaluate the feasibility of perfusion and early-uptake ^{18}F -FDG PET/CT parameters for distinguishing HCC from surrounding liver tissue using a dual-input dual-compartment uptake model and 5 min dynamic PET/CT. Additionally, the usefulness of the derived perfusion and early-uptake ^{18}F -FDG PET/CT imaging for diagnosing HCC was evaluated.

Materials and methods

Patients

This retrospective study was approved by the Institutional Review Board (IRB) of the First People's Hospital of Yunnan (No. 2017YYLH035), and all the methods were performed in accordance with the Declaration of Helsinki. The IRB waived the requirement for informed consent for the deidentified use of medical and radiological data.

Data were collected from a previous study and subsequent clinical practice, and 24 consecutive patients with clinically suspected HCC who had undergone 5 min dynamic ^{18}F -FDG PET/CT and conventional ^{18}F -FDG PET/CT before treatment at Nanfang PET Center, Nanfang Hospital of Southern Medical University from April 2013 to January 2020 were retrospectively enrolled. Patients were included if they had a pathological diagnosis of HCC. Patients were excluded if they had a pathological diagnosis of non-HCC, a lack of pathological diagnosis or suboptimal imaging quality.

We enrolled 15 patients (14 men and one woman) with pathologically confirmed HCC, and the flowchart of the enrolled patients is shown in Fig. 1. Thirteen patients had a single lesion, and two patients had two lesions. Seventeen HCC tumors pathologically confirmed by surgery ($n=11$) or biopsy ($n=6$) were included in this study, and the diameter of these tumors on the longest axis was 6.8 ± 3.8 cm (ranging from 1.4 to 15.0 cm). The subjects had a mean age of 55.5 ± 15.6 years (with an age range of 24–87 years). Thirteen patients were infected with the hepatitis B virus, and 12 patients had liver cirrhosis.

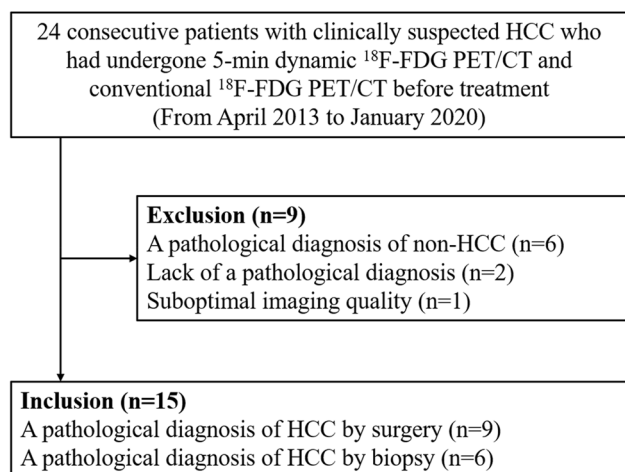


Fig. 1 Flowchart of patients enrolled in this study

PET/CT protocol

^{18}F was produced in a PET tracer cyclotron (GE Healthcare, Waukesha, WI, USA). ^{18}F -FDG was automatically synthesized in a chemical synthesis module (Beijing PET Biotechnology Co., Ltd., China) and had a radiochemical purity of $>95\%$. All the examinations were performed using a Biograph mCTx PET/CT Scanner (Siemens AG, Munich, Germany). The voxel size of the PET system was $2.0364 \times 2.0364 \times 2.027 \text{ mm}^3$.

Early dynamic PET/CT scan

Five-min dynamic PET/CT is used as a supplementary method to conventional PET to diagnose HCC in our clinical settings, and the protocol has been described in a previous study [6]. Briefly, after the patient fasted for more than 6 h and his or her blood glucose was verified, a low-dose liver CT scan (120 kV; 100 mAs) was performed in a single bed position. Next, a 5-min dynamic PET scan was performed concurrently with the administration of the ^{18}F -FDG bolus as described in a previous study [7]. We made several changes: 5-min list-mode data were acquired at early dynamic PET, and ^{18}F -FDG (5.5 MBq/kg) was manually administered as soon as possible in 1 s as a 2 mL bolus in 0.9% saline, followed by 20 mL of 0.9% saline at 2 mL/s for washout.

Although the ideal sampling and image acquisition solution is to divide the scanning time into the shortest intervals possible, the signal-to-noise ratio (SNR) decreases significantly for short PET image acquisition times. Additionally, the standardized uptake value changes considerably in the first 60 s, fluctuates slightly and becomes flat [5]. Thus, the data were reconstructed into 12 sequential frames of 5 s and

4 sequential frames of 60 s each, and 16 sequential frames were obtained.

Conventional PET/CT scan

A whole-body CT scan (120 kV; 200 mAs), including 6–8 bed positions, was performed approximately 60 min after the ^{18}F -FDG bolus injection, and then a PET scan was performed for 1.5 min in each bed position.

Image reconstruction and fusion

All the CT images were reconstructed onto a 512×512 matrix using a filtered back-projection algorithm. Based on the CT data for attenuation correction, all the PET images were reconstructed onto a 200×200 matrix by ordered subset expectation maximization. Image registration was manually performed on transverse, coronal, and sagittal images for each frame of early dynamic PET/CT and conventional PET/CT to minimize the effect of respiratory motion as much as possible.

Standardized uptake value (SUV)

Compared with the mean SUV (SUV_{mean}), the maximum SUV (SUV_{max}) shows significantly improved reproducibility, because it has little to no dependence on region of interest (ROI) demarcation [14], and it performs well for characterizing blood flow in HCC, because it is less susceptible to tumor heterogeneity [5]; thus, SUV_{max} was used in this study. To avoid confusion, we used the term “ SUV_{max} ” to refer to ^{18}F -FDG uptake in conventional PET/CT, while the term “ $dSUV_{max}$ ” was used in 5-min dynamic PET/CT. Both SUV_{max} and $dSUV_{max}$ were manually measured from PET/CT fusion images by placing ROIs.

Data processing and parameter calculation

Time–activity curve (TAC)

The TACs were generated from the $dSUV_{max}$ of each ROI, including the HCC, surrounding liver tissue, aorta and portal vein, from the total of 16 sequential frames in 5-min dynamic PET/CT. The area of the ROI of the dual-input was approximately two-thirds of its vascular cross-section placed on the abdominal aorta and main portal vein. The identification of tumors for ROI placement was performed according to early dynamic, conventional PET/CT and/or other imaging modalities. The respective ROI was placed on the surrounding tumor-free liver tissue to avoid blood vessels.

A large quantity of data are required to make the model calculation work well; thus, linear interpolation processing was performed according to the collected image data [15].

Dual-input dual-compartment model uptake method

The ¹⁸F-FDG activity curve is fitted to a dual-input dual-compartment uptake model as proposed by Sourbron et al. [16] in the quantification of liver perfusion and function with Gd-EOB-DTPA MR. ¹⁸F-FDG and Gd-EOB-DTPA are intracellular contrast agents and have comparable imaging findings of extracellular agents in the arterial and portal venous phases [17, 18]. The dual-input two-compartment uptake model is defined by four tissue parameters (hepatic arterial blood flow *F_a*, portal vein blood flow *F_v*, blood volume *BV* and intracellular uptake rate *K_i*) [13, 16]. Two optional large-vessel delay times (arterial delay *T_a* and portal venous delay *T_v*) were used in this model. *T_a* and *T_v* were fixed at 0–5 s, and each possible value was optimized to achieve the best fit (or the smallest residuals) [13].

The derived parameters are the total blood flow *F* (*F_a* + *F_v*), extracellular mean transit time *MTT* (*BV* / [*F_a* + *F_v* + *K_i*]), *HPI* (*F_a* / [*F_a* + *F_v*]), and portal vein perfusion index *PPI* (*F_v* / [*F_a* + *F_v*]).

Expressing the conservation of the tracer mass in each compartment leads to the following formulas:

$$BV \frac{dC_e}{dt}(t) = F_a C_a(t - T_a) + F_v C_v(t - T_v) - (F_a + F_v + K_i) C_e(t)$$

$$V_i \frac{dC_i}{dt}(t) = K_i C_e(t)$$

$$f_i = K_i / (F_a + F_v + K_i)$$

$$T_e = BV / (F_a + F_v + K_i),$$

where *C_e* and *C_i* represent the tracer concentrations in the extracellular and intracellular compartments, respectively; *C_a* and *C_v* represent the arterial input function and portal venous input function, which are the tracer concentrations in the aorta and portal vein, respectively [13, 16]; *f_i* represents the intracellular uptake fraction; and *T_e* represents the *MTT*.

The formula can be derived as follows:

$$C(t) = [T_e \delta(t) + f_i] \times \frac{e^{-\frac{t}{T_e}}}{T_e} \times [F_a C_a(t - T_a) + F_v C_v(t - T_v)],$$

where $\delta(t)$ indicates the impulse function. It is a singular function and a type of idealized mathematical model with extremely strong intensity, a short time of action and limited integration [19]. The impulse function is defined as follows:

$$\delta(t) = \begin{cases} \infty & t = 0 \\ 0 & t \neq 0 \end{cases}$$

In general, the unit impulse function satisfies the following conditions:

$$\text{When } t \neq 0, \delta(t) = 0, \text{ and } \int_{-\infty}^{+\infty} \delta(t) dt = 1.$$

Fitting calculation

A fitting method known as the ‘black-box’ method was used to calculate the tissue perfusion and early-uptake parameters in this study [20]. Thus, the input and output of this function can be extracted from the image, but the parameters are unknown and must be calculated. The black-box method helps minimize the difference between the calculated value and real value.

The least-squares fitting algorithm was used to implement the fitting method, leading to the following formula [21, 22]:

$$S(p) = \sum_{i=1}^M [y_i - f(x_i, p)]^2.$$

In the SciPy ‘optimize’ module, *Leastsq* () can be used to perform a least squares fit calculation on the data. *Leastsq* () simply requires the function that calculates the difference and original values of the parameters to be determined. After the fitting is finished, the parameter value obtained is the case that best matches the model formula.

The goodness of fit (*R*) for nonlinear regression was used to evaluate the fitting quality, leading to the following formula [23]:

$$R = 1 - \left(\frac{\sum (y - \hat{y})^2}{\sum y^2} \right)^{1/2},$$

where *y* represents the initial data and \hat{y} represents the fitted data.

Parameter images

Because of the lack of available commercial software, a software package for parameter images was built in PyCharm Professional 2019.3.3 (JetBrains, Prague, Czech Republic) and Photoshop CC 2019 V20.0.0 (Adobe Company, San Jose, United States). The aorta and portal vein were drawn as ROIs for the arterial input function and portal venous input function, respectively, and the formulas for calculating the parameters were as described above.

Using the software package, *F_a*, *HPI*, *MTT* and *K_i* images were generated by performing 16 sequential frames of dynamic PET on a 128 × 128-pixel matrix image for each HCC. Pseudocolor was used for parameter images to display the calculated value in each pixel. The PET/CT parameter images were obtained by fusing these parameter images with the CT images.

Imaging quality

The imaging quality was evaluated using the signal-to-noise ratio (SNR) in the liver defined by the following formula [24]:

$$SNR = SUV_{ave}/SUV_{SD},$$

where SUV_{ave} is the average of SUV and SUV_{SD} is the standard deviation of SUV . The 31–35 s dynamic PET image was used to evaluate the imaging quality of early 5 s dynamic PET because it is the earliest frame warranting a measurable amount of ^{18}F -FDG in the liver in all the patients. To evaluate the imaging quality of parameter images, the SUV was replaced by the gray value.

Visual analysis

The identification of HCC for each parameter imaging and conventional PET/CT imaging was reported independently by two nuclear medicine physicians who did not know the clinical data or other imaging information. If the two physicians disagreed, a final consensus was reached after consultation.

HCC lesions were identified as areas of focal increased pseudocolor value exceeding that of the surrounding liver tissue in the Fa , HPI and Ki parameter images and focal decreased pseudocolor value exceeding that of the surrounding liver tissue in the MTT parameter images. HCCs were identified as areas of focal increased uptake exceeding that of the surrounding liver tissue in the conventional PET/CT images. CT imaging was used to determine the exact location of the lesion.

Statistical analysis

The derived parameters and SUV_{max} were compared between HCC and surrounding liver tissue using receiver operating characteristic (ROC) curve analysis. The diagnostic performance for differentiating HCC from the surrounding liver tissue was compared between the derived parameters and SUV_{max} using ROC curve analysis. The interrater agreement test was used to evaluate the visual analysis from the two readers, and the diagnostic concordance was considered statistically significant if the $kappa$ value was >0.750 . The McNemar test was used to compare the positive findings between perfusion and early-uptake PET/CT alone, conventional PET/CT alone and the combined method. If $P < 0.05$, the difference was considered statistically significant. Statistical analyses were performed using MedCalc, version 13.0.0.0 (MedCalc Software, Ostend, Belgium).

Results

Imaging and fitting quality

Imaging quality

The liver was clearly identified in all 15 patients in early 5-s dynamic PET/CT and parameter images, and Fig. 2a–c shows an example in a patient. The liver SNRs of early 5-s dynamic PET and parameter images are shown in Table 1.

Fitting quality

The fitted data matched well with the original data for all 17 HCC tumors ($R = 0.881 \pm 0.029$) and 15 surrounding liver tissues ($R = 0.905 \pm 0.033$). Figure 2d shows an example of the fitted and original curves of HCC and the surrounding liver tissue in a patient.

Perfusion, early-uptake and conventional PET/CT parameters

The perfusion and early-uptake parameters and SUV_{max} of PET/CT in HCC and the surrounding liver tissue are shown in Table 2. HCC tumors showed a higher Fa ($P < 0.001$), higher HPI ($P < 0.001$), lower Fv ($P = 0.017$) and lower PPI ($P < 0.001$) than the surrounding liver tissue. F was increased in HCC tumors compared with that in the surrounding liver tissue, but the difference was not statistically significant ($P = 0.155$).

BV was increased and MTT was decreased in HCC tumors compared with those in the surrounding liver tissue, but these differences were not statistically significant ($P = 0.756$ and $P = 0.221$, respectively). Ki was increased in HCC tumors compared with that in the surrounding liver tissue ($P < 0.001$). The SUV_{max} was higher in HCC tumors than that in the surrounding liver tissues ($P < 0.001$).

Compared with the SUV_{max} , Fa , HPI and PPI had significantly improved diagnostic performance ($P = 0.016$, $P = 0.014$ and $P = 0.014$, respectively), BV had significantly poorer diagnostic performance ($P = 0.034$), and Fv , F , Ki and MTT showed no significant difference in the diagnostic performance ($P = 0.806$, $P = 0.317$, $P = 0.057$, $P = 0.650$ and $P = 0.252$, respectively).

Parameter and conventional PET/CT images

All the Fa , HPI , MTT and Ki images from the 17 HCCs were generated and fused with the CT images, one image per patient was used for visual analysis, and the image with the largest diameter of the tumor was selected. The concordance

Fig. 2 Example of imaging and fitting quality of hepatocellular carcinoma (HCC) (marked with long arrow) and surrounding liver tissue (short arrow) in a patient. **a** HCC showed areas of decreased opacity compared with the surrounding liver tissue on nonenhanced CT. **b** The liver can be clearly identified, and HCC showed increased ^{18}F -FDG accumulation compared with the surrounding liver tissue on early 5 s (31–35 s) dynamic PET/CT. **c** The liver can be clearly identified, and HCC showed increased *Fa* and *HPI*, decreased *MTT* and slightly increased *Ki* compared with the surrounding liver tissue in parameter images. **d** The original curve is drawn from the measured values with linear interpolation processing, and the fitted curve (green dotted line) matched well with the original curve (red line) in HCC and the surrounding liver tissue

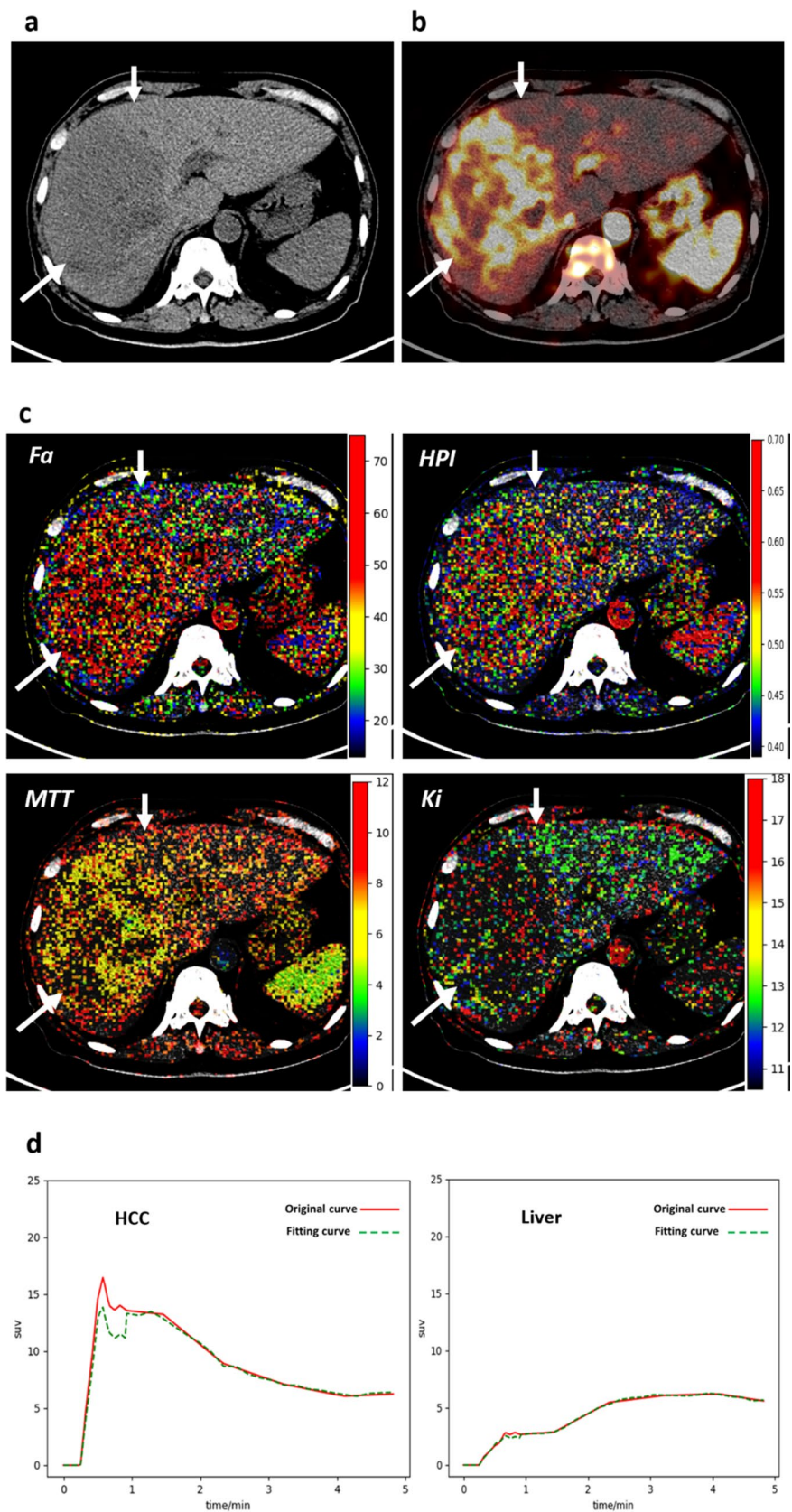


Table 1 Signal-to-noise ratio (SNR) in the liver of the early 5 s (31–35 s) PET and parameter images

Imaging	SNR
Early 5 s PET (31–35 s)	2.9 ± 1.2
Parameter imaging	
<i>Fa</i>	7.7 ± 5.1
<i>HPI</i>	5.6 ± 2.7
<i>MTT</i>	6.8 ± 3.4
<i>Ki</i>	5.6 ± 2.4

Table 2 Perfusion and early-uptake parameters and the maximum standard uptake value (SUVmax) of ¹⁸F-FDG PET/CT between primary hepatocellular carcinoma (HCC) and surrounding liver tissue

Parameter	HCC <i>n</i> = 17	Liver tissue <i>n</i> = 15	AUC	<i>P</i>
<i>Fa</i> (mL/min/100 mL)	85.6 ± 19.4	26.1 ± 14.6	0.988	< 0.001
<i>Fv</i> (mL/min/100 mL)	18.4 ± 8.9	54.5 ± 34.8	0.751	0.017
<i>F</i> (mL/min/100 mL)	104.1 ± 17.4	80.6 ± 40.0	0.655	0.155
<i>HPI</i> (%)	81.7 ± 9.8	37.9 ± 18.5	0.984	< 0.001
<i>PPI</i> (%)	18.3 ± 9.8	59.9 ± 18.3	0.984	< 0.001
<i>BV</i> (mL/100 mL)	24.3 ± 4.1	21.6 ± 8.1	0.535	0.756
<i>MTT</i> (s)	11.8 ± 1.6	13.7 ± 4.2	0.633	0.221
<i>Ki</i> (/100/min)	19.5 ± 1.0	18.6 ± 0.8	0.847	< 0.001
<i>SUV max</i>	5.3 ± 3.5	2.6 ± 0.6	0.786	< 0.001

AUC area under the curve

between the two readers was strong for these parameter images, with a kappa value of 0.882. The results of perfusion and early-uptake PET/CT and conventional PET/CT for identifying HCC as reported by the two readers are shown in Table 3.

Among these 17 HCC lesions, eight (47.1%), eleven (64.7%), nine (52.9%), and seven (41.2%) positive findings were obtained on *Fa*, *HPI*, *MTT*, and *Ki* PET/CT images, respectively. Twelve (70.6%) positive findings were obtained on the total parameter images, and nine (52.9%) positive findings were detected on conventional PET/CT (*P* = 0.508); parameter images detected six (35.3%) HCC tumors that were negative on conventional PET/CT (Fig. 3). Using perfusion and early-uptake PET/CT, the positive rate of an HCC diagnosis was enhanced from 52.9% on conventional PET/CT to 88.2% using the combined method (*P* = 0.031).

Discussion

This study preliminarily demonstrated the feasibility of perfusion and early-uptake ¹⁸F-FDG PET/CT in HCC using 5-min dynamic ¹⁸F-FDG PET/CT and a dual-input dual-compartment uptake model. Compared with previous studies

Table 3 Identification of parameter imaging and conventional PET/CT reported by the two readers in 17 hepatocellular carcinoma (HCC) lesions

HCCs (<i>n</i>)	Perfusion and early-uptake PET/CT				Conventional PET/CT
	<i>Fa</i>	<i>HPI</i>	<i>MTT</i>	<i>Ki</i>	
3	+	+	+	+	+
2	+	+	+	+	-
1	+	+	+	±	-
1	+	+	-	-	+
1	-/+	-/+	-	-	-
1	-	+	+	+	+
1	-	+	+	-	-
1	-	+	-	-	-
1	-	-	+	-	+
3	-	-	-	-	+
2	-	-	-	-	-

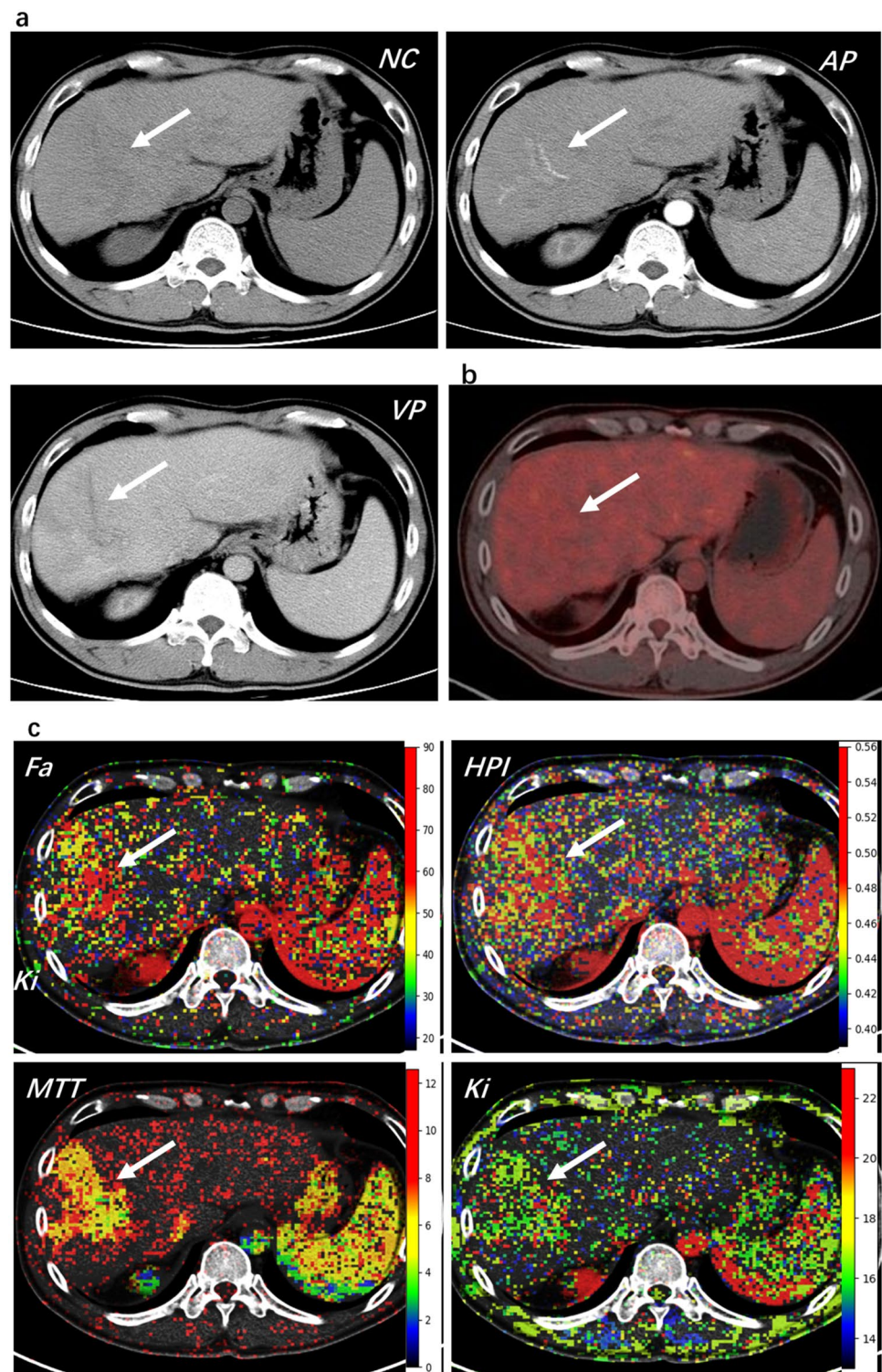
“+” represents positive findings reported by both readers, “-” represents negative findings reported by both readers, “±” represents positive findings reported by reader 1 and negative findings reported by reader 2, and “-/+” represents negative findings reported by reader 1 and positive findings reported by reader 2

that used other analytic methods to estimate ¹⁸F-FDG transport [7, 11, 25], this study presented additional parameters and preliminarily generated parameter images to diagnose HCC. The image quality of the 5 s frame of dynamic PET/CT and parameter images met the requirements of data measurement and visual analysis. Curve fitting performed well in HCC tumors and surrounding liver tissues. The results of parameter images to detect HCC showed a strong concordance between the two readers (kappa value > 0.750), ensuring diagnostic reproducibility.

Time-consuming dynamic PET/CT is impractical in a busy clinical setting and has a poor patient tolerance, and some researchers have begun to explore short-term dynamic PET to assess ¹⁸F-FDG dynamics in recent years. Winterdahl et al. [26] demonstrated that 3-min dynamic ¹⁸F-FDG PET data could be used to estimate liver blood perfusion in pigs. Using the maximum-slope method, Bernstine et al. [7] demonstrated that 1.5-min dynamic ¹⁸F-FDG PET-derived blood flow parameters could be used to help distinguish and characterize HCCs. Samimi et al. [27] also found that a 5-min short duration with static PET/CT data after 60 min achieved a strong correlation between all pharmacokinetic parameters from 60-min full scanning. A 5-min dynamic PET was used in this study, because *Ki* was calculated and reflected intracellular FDG uptake, which takes more time than the blood flow dose.

HCC has a blood supply mainly derived from the hepatic artery than the portal vein. Compared with the surrounding liver tissue, HCCs had higher *Fa* and *HPI* and lower *Fv* and *PPI*, according to previous studies that

Fig. 3 Parameter images identify primary hepatocellular carcinoma (marked with arrows) with negative findings on conventional PET/CT. **a** Nonenhanced (NE) CT showed areas of slightly decreased opacity in the right lobe of the liver; the arterial phase (AP) of enhanced CT showed abnormal vascular enhancement, and the venous phase showed slightly heterogeneous enhancement. **b** Conventional PET/CT showed negative findings in the liver. **c** Parameter imaging showed areas of increased *Fa*, *HPI* and *Ki* and decreased *MTT* compared with that in the surrounding liver tissue



used CT and MR with extracellular agents for liver perfusion imaging [2, 10, 28, 29]. This study achieved similar results: HCC had a significantly higher *Fa* and *HPI* (both $P < 0.001$), slightly higher *F* ($P > 0.05$) and significantly lower *Fv* ($P < 0.05$) and *PPI* ($P < 0.001$) than the surrounding liver tissues.

Angiogenesis is a hallmark of HCC development and progression, and microvascular density has been considered an index of angiogenesis [3]. Tumor microvascular density is more closely related to *BV* than to blood flow because blood flow, in the absence of an autoregulatory mechanism (which is underdeveloped in tumor vessels), can be easily affected

by cardiac output, but not blood volume [2, 3]. Unfortunately, BV was not significantly different in HCC tumors compared with that in the surrounding liver tissue in this study ($P > 0.05$). However, BV might serve as an index for treatment response evaluation. Taouli et al. [28] demonstrated that BV did not significantly differ between untreated HCCs and the surrounding liver tissue but did differ between treated HCCs and the surrounding liver tissue.

Decreased MTT usually reflects the presence of arteriovenous shunts, which are frequently observed in HCC tumors. Sahani et al. [30] demonstrated that MTT was significantly decreased in HCC compared with that in the surrounding liver tissue, but no significant difference was reported by Taouli et al. [28]. Our results showed that MTT was slightly lower in HCC tumors than in the surrounding liver tissue ($P > 0.05$).

Ki is directly proportional to tissue glucose metabolism, independent of body habitus or uptake period, and is superior to SUV as an indicator of FDG uptake by tumors [31]. Ki is commonly estimated using a 60-min dynamic PET/CT scan, and both simulated and clinical results indicated enhanced Ki in tumors compared with that in surrounding liver tissues based on the different pharmacokinetic models [32]. In this study, Ki is considered an index for reflecting the early uptake of ^{18}F -FDG. Our results demonstrated a significant increase in Ki in HCC tumors using a time-saving 5-min dynamic PET/CT scan ($P < 0.001$). For conventional PET/CT, the results showed a higher SUVmax in HCC tumors than in the surrounding liver tissue ($P < 0.001$).

^{18}F -FDG is transported into cells and phosphorylated to FDG-6-phosphate, which is trapped within cells. However, the positive rate of an HCC diagnosis on ^{18}F -FDG PET/CT is only 36–70%, because moderately differentiated or well-differentiated HCC commonly has high FDG-6-phosphatase activity and high expression of P-glycoprotein, which transports the tracer out of the cells, and certain subtypes of HCC have reduced uptake of FDG because of the low expression of glucose transporter (Glut)-1 or Glut-2 [4, 33].

This study demonstrated that certain functional parameters from perfusion and early-uptake ^{18}F -FDG PET/CT performed better than SUVmax from conventional ^{18}F -FDG PET/CT for differentiating HCC from background liver tissue. Compared with SUVmax, Fa , HPI and PPI had significantly improved diagnostic performances (all $P < 0.05$), Fv , F , Ki and MTT showed no significant difference (all $P > 0.05$), and BV had a significantly poorer diagnostic performance ($P < 0.05$). These results are in concordance with the visual analysis from the two readers that perfusion and early-uptake ^{18}F -FDG PET/CT images achieved a slightly higher positive positivity rate than conventional ^{18}F -FDG PET/CT ($P > 0.05$).

Among the HCC lesions, 70.6% were positive on perfusion and early-uptake ^{18}F -FDG PET/CT images, similar to

the results of enhanced CT for diagnosing HCC, which has a sensitivity of 54% and 78% in the early and later arterial phases, respectively [34]. A possible reason for the diagnosis of these HCC lesions with negative findings on the parameter images is the inclusion of certain lesions with a poor blood supply and/or small size in this study. Additionally, parametric images are noisy and may interfere with the diagnosis.

Interestingly, perfusion and early-uptake PET/CT detected 35.3% of HCC lesions with negative findings on conventional PET/CT. Overall, the positive rate of an HCC diagnosis was enhanced from 52.9% on conventional PET/CT to 88.2% ($P < 0.05$). Thus, perfusion and early-uptake PET/CT might serve as additional functional imaging to solve the clinical dilemma of the low sensitivity of conventional ^{18}F -FDG PET/CT for HCC diagnosis. Concurrent evaluation of blood flow dynamic status and metabolic activity may improve the role of PET/CT in the diagnosis of HCC.

This study has some limitations. First, the sample size of the dataset was small; second, an analysis of the relationship between the tumor biological characteristics and these parameters is lacking because of the retrospective nature of the study; third, further studies must determine the role of perfusion and early-uptake PET/CT for characterizing the tumor biological characteristics, evaluating anticancer therapy efficacy, predicting early responses to anticancer treatment and other diagnostic applications; fourth, parametric images of the liver are noisy, which may obscure or mimic the tumor, and the tumor boundary is not clear in these parametric images, but improvements in the sensitivity of PET/CT scanner, dynamic image reconstruction postprocessing technology, and parametric imaging software or the increase in the ^{18}F -FDG dose may help reduce these limitations; fifth, dynamic scanning requires extra occupation of the PET/CT scanner; sixth, the statistical noise causes an undesirable increase in dSUVmax, and these dynamic images have different noise properties, presumably leading to different degrees of overestimation of the true radioactivity and, consequently, the deformation of the curve.

Conclusions

We proposed a feasible method to estimate HCC perfusion and early uptake using 5-min dynamic ^{18}F -FDG PET/CT and a dual-input dual-compartment uptake model. Perfusion and early-uptake PET/CT are useful and provide additional functional information to diagnose HCC. This study introduced the promising concept of integrating perfusion PET/CT with metabolic PET/CT to enhance the HCC diagnosis.

Author contributions SW and BL analyzed the data and wrote the manuscript, and the other authors helped to search the literature; PL and RX measured the data; SW and QW performed imaging analysis; and HS and JH critically revised the manuscript for important intellectual content and approved the final version of the article to be published.

Funding (1) Basic Research on Application of Joint Special Funding of Science and Technology Department of Yunnan Province-Kunming Medical University, No. 2018FE001(-291); (2) National Natural Science Foundation of China, No. 81760306; (3) High-level Talent Project of Health in Yunnan Province, No. D-2018011; (4) Ten Thousand People Plan in Yunnan Province, No. YNWR-QNBJ-2018-243.

Declarations

Conflict of interest The authors declared that they have no conflicts of interest.

Ethical approval This study was approved by the Institutional Review Board (IRB) of the First People's Hospital of Yunnan (No. 2017YYLH035). All procedures performed in studies involving human participants were in accordance with the ethical standards of the institutional and/or national research committee and with the 1964 Helsinki Declaration and its later amendments or comparable ethical standards.

Informed consent The IRB waived the requirement for informed consent for the deidentified use of medical and radiological data.

References

- Bray F, Ferlay J, Soerjomataram I, Siegel RL, Torre LA, Jemal A. Global cancer statistics 2018: GLOBOCAN estimates of incidence and mortality worldwide for 36 cancers in 185 countries. *CA Cancer J Clin*. 2018;68(6):394–424.
- Kim SH, Kamaya A, Willmann JK. CT perfusion of the liver: principles and applications in oncology. *Radiology*. 2014;272(2):322–44.
- Chen J, Chen C, Xia C, Huang Z, Zuo P, Stemmer A, et al. Quantitative free-breathing dynamic contrast-enhanced MRI in hepatocellular carcinoma using gadoxetic acid: correlations with Ki67 proliferation status, histological grades, and microvascular density. *Abdominal Radiology*. 2017;43(6):1393–403.
- Lu RC, She B, Gao WT, Ji YH, Xu DD, Wang QS, et al. Positron-emission tomography for hepatocellular carcinoma: current status and future prospects. *World J Gastroenterol*. 2019;25(32):4682–95.
- Schierz JH, Opfermann T, Steenbeck J, Lopatta E, Settmacher U, Stallmach A, et al. Early dynamic 18F-FDG PET to detect hyperperfusion in hepatocellular carcinoma liver lesions. *J Nucl Med*. 2013;54(6):848–54.
- Wang SB, Wu HB, Wang QS, Zhou WL, Tian Y, Li HS, et al. Combined early dynamic (18)F-FDG PET/CT and conventional whole-body (18)F-FDG PET/CT provide one-stop imaging for detecting hepatocellular carcinoma. *Clin Res Hepatol Gastroenterol*. 2015;39(3):324–30.
- Bernstine H, Braun M, Yefremov N, Lamash Y, Carmi R, Stern D, et al. FDG PET/CT early dynamic blood flow and late standardized uptake value determination in hepatocellular carcinoma. *Radiology*. 2011;260(2):503–10.
- Etard C, Celier D, Roch P, Aubert B. National survey of patient doses from whole-body FDG PET-CT examinations in France in 2011. *Radiat Prot Dosimetry*. 2012;152(4):334–8.
- Frampas E, Lassau N, Zappa M, Vullierme MP, Koscielny S, Vilgrain V. Advanced hepatocellular carcinoma: early evaluation of response to targeted therapy and prognostic value of perfusion CT and dynamic contrast enhanced-ultrasound. Preliminary results *Eur J Radiol*. 2013;82(5):e205–11.
- Jajamovich GH, Huang W, Besa C, Li X, Afzal A, Dyvorne HA, et al. DCE-MRI of hepatocellular carcinoma: perfusion quantification with Tofts model versus shutter-speed model—initial experience. *Magn Reson Mater Phys, Biol Med*. 2015;29(1):49–58.
- Mullani NA, Herbst RS, O'Neil RG, Gould KL, Barron BJ, Abbruzzese JL. Tumor blood flow measured by PET dynamic imaging of first-pass 18F-FDG uptake: a comparison with 15O-labeled water-measured blood flow. *J Nucl Med*. 2008;49(4):517–23.
- Mullani NA, Gould KL. First-pass measurements of regional blood flow with external detectors. *J Nucl Med*. 1983;24(7):577–81.
- Chandarana H, Block TK, Ream J, Mikheev A, Sigal SH, Otazo R, et al. Estimating liver perfusion from free-breathing continuously acquired dynamic gadolinium-ethoxybenzyl-diethylenetriamine pentaacetic acid-enhanced acquisition with compressed sensing reconstruction. *Invest Radiol*. 2015;50(2):88–94.
- Kinahan PE, Fletcher JW. Positron emission tomography-computed tomography standardized uptake values in clinical practice and assessing response to therapy. *Semin Ultrasound CT MR*. 2010;31(6):496–505.
- Thirion JP. Fast non-rigid matching of 3D medical images. *INRIA, RR-2547*; 1995.
- Sourbron S, Sommer WH, Reiser MF, Zech CJ. Combined quantification of liver perfusion and function with dynamic gadoxetic acid-enhanced MR imaging. *Radiology*. 2012;263(3):874–83.
- Freesmeyer M, Winkens T, Schierz JH. Contrast between hypervascularized liver lesions and hepatic parenchyma: early dynamic PET versus contrast-enhanced CT. *Ann Nucl Med*. 2014;28(7):664–8.
- Huppertz A, Haraida S, Kraus A, Zech CJ, Scheidler J, Breuer J, et al. Enhancement of focal liver lesions at gadoxetic acid-enhanced MR imaging: correlation with histopathologic findings and spiral CT—initial observations. *Radiology*. 2005;234(2):468–78.
- Sourbron S, Ingrisch M, Siefert A, Reiser M, Herrmann K. Quantification of cerebral blood flow, cerebral blood volume, and blood-brain-barrier leakage with DCE-MRI. *Magn Reson Med*. 2009;62(1):205–17.
- Vanhuffel S, Chen H, Decanniere C, Vanhecke P. Algorithm for time-domain NMR data fitting based on total least squares. *J Magn Reson, Ser A*. 1994;110(2):228–37.
- Pilu M, Fisher RB, Fitzgibbon A. Direct least square fitting of ellipses. *IEEE Trans Pattern Anal Mach Intell*. 1999;21(5):476–80.
- Komatsu D, Yamada A, Suzuki T, Kurozumi M, Fujinaga Y, Ueda K, et al. Compartment model analysis of intravenous contrast-enhanced dynamic computed tomography in hepatic hemodynamics: a validation study using intra-arterial contrast-enhanced computed tomography. *Hepatol Res*. 2018;48(10):829–38.
- Wu J, Zhao C, editors. Cooperation on the Monte Carlo rule: prisoner's dilemma game on the grid. National conference of theoretical computer science. Springer; 2019.
- Hartung-Knemeyer V, Beiderwellen KJ, Buchbender C, Kuehl H, Lauenstein TC, Bockisch A, et al. Optimizing positron emission tomography image acquisition protocols in integrated positron emission tomography/magnetic resonance imaging. *Invest Radiol*. 2013;48(5):290–4.
- Geist BK, Wang J, Wang X, Lin J, Yang X, Zhang H, et al. Comparison of different kinetic models for dynamic 18F-FDG PET/CT imaging of hepatocellular carcinoma with various, also dual-blood input function. *Phys Med Biol*. 2020;65(4):045001.

26. Winterdahl M, Munk OL, Sorensen M, Mortensen FV, Keiding S. Hepatic blood perfusion measured by 3 minute dynamic 18F-FDG PET in pigs. *J Nucl Med.* 2011;52(7):1119–24.
27. Samimi R, Kamali-Asl A, Geramifar P, van den Hoff J, Rahmim A. Short-duration dynamic FDG PET imaging: optimization and clinical application. *Phys Med.* 2020;80:193–200.
28. Taouli B, Johnson RS, Hajdu CH, Oei MT, Merad M, Yee H, et al. Hepatocellular carcinoma: perfusion quantification with dynamic contrast-enhanced MRI. *AJR Am J Roentgenol.* 2013;201(4):795–800.
29. Ippolito D, Querques G, Okolicsanyi S, Franzesi CT, Strazzabosco M, Sironi S. Diagnostic value of dynamic contrast-enhanced CT with perfusion imaging in the quantitative assessment of tumor response to sorafenib in patients with advanced hepatocellular carcinoma: a feasibility study. *Eur J Radiol.* 2017;90:34–41.
30. Sahani DV, Holalkere N-S, Mueller PR, Zhu AX. Advanced hepatocellular carcinoma: CT perfusion of liver and tumor tissue—initial experience. *Radiology.* 2007;243(3):736–43.
31. Sadato N, Tsuchida T, Nakaumra S, Waki A, Uematsu H, Takahashi N, et al. Non-invasive estimation of the net influx constant using the standardized uptake value for quantification of FDG uptake of tumours. *Eur J Nucl Med.* 1998;25(6):559–64.
32. Karakatsanis NA, Lodge MA, Tahari AK, Zhou Y, Wahl RL, Rahmim A. Dynamic whole-body PET parametric imaging: I. Concept, acquisition protocol optimization and clinical application. *Phys Med Biol.* 2013;58(20):7391–418.
33. European Association for the Study of the Liver. Electronic address eee, European association for the study of the L. EASL clinical practice guidelines: management of hepatocellular carcinoma. *J Hepatol.* 2018;69(1):182–236.
34. Murakami T, Kim T, Takamura M, Hori M, Takahashi S, Federle MP, et al. Hypervascular hepatocellular carcinoma: detection with double arterial phase multi-detector row helical CT. *Radiology.* 2001;218(3):763–7.

Publisher's Note Springer Nature remains neutral with regard to jurisdictional claims in published maps and institutional affiliations.